CrystEngComm

Dynamic Article Links

Cite this: *CrystEngComm*, 2011, **13**, 4714

www.rsc.org/crystengcomm

PAPER

Role of ethanol in sodalite crystallization in an ethanol–Na_2O–Al_2O_3–SiO_2–H_2O system†

Yi Huang,[ab] Jianfeng Yao,[a] Xueyi Zhang,[b] Chunhua (Charlie) Kong,[c] Huiyong Chen,[b] Dongxia Liu,[b] Michael Tsapatsis,[b] Matthew R. Hill,[de] Anita J. Hill*[e] and Huanting Wang*[a]

Received 11th February 2011, Accepted 21st April 2011
DOI: 10.1039/c1ce05194f

Crystallization of sodalite was studied in an ethanol–Na_2O–Al_2O_3–SiO_2–H_2O system. The addition of ethanol was observed to significantly affect the crystallization process and final crystal sizes and morphologies. Micron-sized sodalite particles with disc and thread-ball-like shapes were produced at low ethanol contents whereas sodalite particles with core-shell nanostructures were dominant at high ethanol contents. Prolongation of the reaction time led to hollow architectures with polycrystalline shells. This study showed that the formation of core-shell and hollow sodalite structures followed a surface crystallization process, including the following steps: the formation of amorphous spherical aggregates, multiple nucleation on the surface, growth of shell nanocrystals, and amorphous core digestion. The present work provides new insights into a better understanding of the role of ethanol in zeolite crystallization, and controllable synthesis of sodalite crystals with different morphologies.

1. Introduction

Zeolites are a class of microporous crystalline solids with uniform molecular-sized pores and channels (<2 nm), and they are widely used in the areas such as catalysis, ion exchange, separation, and adsorption.[1–7] To better control the sizes and morphologies of zeolite structures, it is important to understand zeolite formation mechanisms including nucleation, crystal growth and assembling processes. To date, zeolite crystallization process in conventional gel systems under hydrothermal conditions has been extensively studied. It has been reported that the crystallization starts with heterogeneous solid-gel surface-catalyzed nucleation accompanied by an increase of the interfacial surface area involved.[8] Therefore, the initial gel microstructures play an important role in controlling crystallization kinetics, such as nucleation and crystal growth rates. This proposed mechanism was supported by the observation of zeolite A nucleation at the solid–liquid interface in a Na_2O–Al_2O_3–SiO_2–H_2O system.[9] A similar phenomenon was also observed in the synthesis of FAU-type zeolite, except that an aggregation mechanism was found to be spontaneous during the crystal growth.[10,11] However, the zeolite nucleation and growth processes are much more complicated when organic additives are involved in the system. The introduction of organic additives of different chemical nature may alter the nucleation and crystal growth behavior due to the interaction between organic and inorganic components in the system. For instance, a surface-to-core crystallization process was recently observed in zeolite A[12,13] and analcime[14] when biopolymer chitosan and ethylamine were introduced, respectively. In the former case, crystallization was first observed on the amorphous particle surface and then extended inwards resulting in a *monocrystalline* zeolite A cube with an amorphous core.[12,13] A similar crystallization process was also observed in the synthesis of other zeolite structures such as hollow sodalite spheres,[15] cubic $AlPO_4$-11,[16] and hierarchical porous zeolite NaP monolith.[17]

Ethanol is a common organic solvent and often involved in the hydrothermal synthesis of zeolites. For instance, ethanol was introduced *via* hydrolysis of tetraethyl orthosilicate (TEOS) in the synthesis of zeolite A,[18] silicalite-1[5,19,20]/ZSM-5,[21–24] and zeolite Y.[25] It is known that adding ethanol in zeolite synthesis solutions slows down zeolite crystallization process, resulting in small crystal sizes.[26] Ethanol was also used in the microemulsion-assisted synthesis of zeolites with controllable morphologies.[27,28] Furthermore, in a zeolite A synthesis gel free of

[a]*Department of Chemical Engineering, Monash University, Clayton, VIC 3800, Australia. E-mail: huanting.wang@monash.edu; Fax: +61-3-9905-5686; Tel: +61-3-9905-3449*
[b]*University of Minnesota, Department of Chemical Engineering and Materials Science, 421 Washington Avenue SE, Minneapolis, MN 55455, USA*
[c]*Electron Microscope Unit, University of New South Wales, Sydney, NSW 2052, Australia*
[d]*School of Chemistry, University of Melbourne, Victoria, 3010, Australia*
[e]*Commonwealth Scientific and Industrial Research Organization (CSIRO) Materials Science and Engineering, Private Bag 33, Clayton South, Victoria, 3169, Australia. E-mail: anita.hill@csiro.au; Fax: + 61-3-9544-1128; Tel: + 61-3-9545-2665*

† Electronic supplementary information (ESI) available. See DOI: 10.1039/c1ce05194f

structure-directing agents, nanocrystalline sodalite was produced when a large amount of ethanol was added.[29] Therefore, the effect of ethanol on zeolite crystallization appears to be quite complex, especially in the systems with excessive ethanol. More study on the effect of ethanol is needed to gain a better understanding of the role of ethanol in the course of zeolite crystallization and morphological evolution.

In this work, we systematically studied the crystallization of sodalite structures with different morphologies in an ethanol–Na_2O–Al_2O_3–SiO_2–H_2O system. In particular, clusters of sodalite discs, spherical aggregates of sodalite nanoplates (*e.g.*, thread-ball-like particles), and core-shell/hollow sodalite structures were synthesized by varying the ethanol content and hydrothermal synthesis time. The detailed investigations of crystallization processes are presented in this paper. Our study provides a new insight into the crystallization of zeolite nanostructures in the ethanol–Na_2O–Al_2O_3–SiO_2–H_2O system, and offers an alternative approach to controlling the crystal sizes and morphologies.

2. Experimental section

Sodalite synthesis

The synthesis of sodalite was performed in an ethanol–Na_2O–Al_2O_3–SiO_2–H_2O system. The synthesis method was similar to that described in our previous study.[29] First, an alkaline solution with a molar composition of $3.61Na_2O : 1.0Al_2O_3 : 43.50H_2O$ was prepared by mixing 5.00 g of sodium hydroxide (99%, Sigma-Aldrich), 4.91 g of sodium aluminate (anhydrous, Sigma-Aldrich), and 20.00 g of doubly deionized (DDI) water. The solution was stirred for 2–3 h until it became clear. Then, 6.50 g of colloidal silica (LUDOX HS-30, 30 wt %, Aldrich) was added, followed by magnetic stirring for 3–5 h to give a homogeneous milky gel with a molar composition of $3.61Na_2O : 1.0Al_2O_3 : 1.20SiO_2 : 52.84H_2O$. Different amounts of ethanol (200 proof, ≥99.5%, Sigma-Aldrich) were added to complete the synthetic mixture, followed by vigorous stirring at room temperature for 24 h. It was observed that even after 24h agitation the zeolite gel still appeared to partition in the bottom forming a two-phase mixture. The final molar composition of the synthesis mixture was $3.61Na_2O : 1.00Al_2O_3 : 1.20SiO_2 : 52.84H_2O : nC_2H_6O$ ($n_{ethanol}$ = 0, 4, 8, 16, 32, and 48, corresponding to the addition of 0, 5, 10, 20, 40, and 60 g of ethanol, respectively.). The synthesis mixture was then transferred into an electrically heated oven for hydrothermal reaction at 90 °C. In order to investigate the crystal growth at different stages, samples were prepared with reaction time of 0.5, 1, 2, 3, 5, 8, 16, 25, 35, 45, and 65 h. Note that for each reaction time, at least 6 different experiments were preformed. The polypropylene (PP) bottles containing samples were then cooled down by running tap water for 5 min. The products were repeatedly washed with DDI water using filtration until a pH value of ~7 was reached, and then dried at 90 °C for 12 h. The control experiment was carried out using the same procedures, except that 20 g of water instead of ethanol was added to the freshly prepared zeolite gel before further agitation. The control system has a final molar composition of $3.61Na_2O : 1.00Al_2O_3 : 94H_2O$.

The specimens synthesized in the ethanol–Na_2O–Al_2O_3–SiO_2–H_2O system and control experiment were designated SOD-*n*Et(*t*) and LTA-*n*Wt(*t*), respectively, where "Et" stands for ethanol, "Wt" represents water, "*n*" represents the molar composition of ethanol ($n_{ethanol}$) or water (n_{water}) in the system, and "*t*" represents reaction time in hours. For example, SOD-16Et(3) denotes a sodalite sample prepared after 3 h hydrothermal reaction in the system with a mole composition of $3.61Na_2O : 1.0Al_2O_3 : 1.20SiO_2 : 52.84H_2O : 16C_2H_6O$.

Characterization

X-ray powder diffraction (XRD) analysis was conducted using a Philips PW1140/90 diffractometer with a Cu-Kα target (40 kV, 25 mA), at a scan rate of 1°/min and a step size of 0.02. IR spectra were recorded on a Perkin–Elmer Spectrum 100 FT-IR spectrometer with samples pressed in KBr pellets. Thermogravimetric analysis (TGA) measurements were performed in flowing air or nitrogen at a flowrate of 20 mL min^{-1} in a Pt pan, on a Perkin-Elmer Pyris 1 Analyzer in the range of 20–700 °C with a heating rate of 5 °C min^{-1}. To ensure consistency in mass loss profiles, all samples were equilibrated for 60 s under the relevant gas stream prior to commencement of the analysis. The specimens were dried at 100 °C for 24 h before TGA analysis. Morphology of the specimens was examined using scanning electron microscopy (SEM) on a JEOL Model JSM-6500FE scanning electron microscope operated at 5–15 kV.

The cross-sectional SEM images of the zeolite samples were taken using a FEI Nova xT Nanolab 200 Dualbeam focused ion beam (FIB) combined with a field emission scanning electron microscope (FESEM). In order to achieve stable and conductive working conditions in the FIB-FESEM, a single layer of zeolite powder was dispersed and fixed on the top of a standard SEM stub facilitated with the double-sided carbon sticker tab. The loose and excess particles were removed from the carbon tab by shaking and knocking on the edge of the stub upside down. A thin layer of Au about 40 nm was coated on the prepared sample with an Emitech K550x sputter coater. In the Dualbeam FIB-FESEM, a few typical particles of zeolite were selected for cross-sectional analysis. One half of the selected spherical or cubic shaped particle was carefully removed by the focused ion beam, and the cross section of the remaining half of the particle was polished with a finer ion beam and then scanned for secondary electron imaging.

The TEM samples for particles were prepared by applying a few droplets of aqueous suspension of the particles onto a copper grid coated with carbon (Ted Pella Inc.). The grid was then allowed to air dry. The TEM samples for thin sections were prepared by embedding the particles in epoxy resin, followed by sectioning using a Leica EM UC6 microtome. The thickness of the slices was around ~70 nm. The sections were mounted on a copper mesh grid for subsequent transmission electron microscopy (TEM) investigation, which was conducted on an FEI Tecnai G2 F30 transmission electron microscope operating at 300 kV, and an FEI Tecnai T12 transmission electron microscope operating at 120 kV. All TEM images were recorded using a CCD camera.

3. Results and discussion

The synthesis conditions as well as the initial composition of the synthesis precursor are summarized in Table 1. To monitor the zeolite crystallization in each system, samples were collected after reaction times of 1, 2, 3, 5, 8, 16, 25, 45, and 65 h. The zeolite phases present in each sample (determined by XRD) are also summarized in Table 1. As can be seen, zeolite A is more stable in the water solvent system. However, upon the addition of ethanol, the phase transformation from zeolite A to sodalite is considerably accelerated. According to Table 1, a shorter phase transformation period was observed for the system with increasing ethanol content, indicating that the system with more ethanol favors the crystallization of sodalite under the current hydrothermal conditions.

In the following we will mainly focus on samples after reaction times of 3 and 5 h to illustrate the effect of ethanol content on zeolite A/sodalite crystallization. However, samples synthesized from the representative system with a molar composition of $16C_2H_5OH$–$3.61Na_2O$–$1Al_2O_3$–$1.20SiO_2$–$52.84H_2O$ throughout 1 and 65 h reaction times will also be presented and discussed in order to describe the sequence of events that lead to hollow sodalite particle formation.

Effects of ethanol content

By varying the ethanol content in the system, sodalites with different morphologies and size distributions were synthesized.

XRD patterns of representative samples are shown in Fig. 1. In the system with only water as solvent, pure zeolite A (LTA-94Wt(3)) was crystallized after a reaction time of 3 h. As shown in Fig. 1a, the characteristic zeolite A XRD peaks can be indexed to the face-centered cubic unit cell with dimensions $a = 24.61$ Å, matching the standard structural data provided by the International Zeolite Association.[30] Under the same reaction condition and without addition of extra water and ethanol (SOD-0Et(3)), some sodalites are observed (as indicated by arrows in Fig. 1b). This is because without addition of extra water the synthesis zeolite gel became more concentrated, and a higher concentration of sodium ion and pH favored sodalite crystallization.[31,32] Extending the reaction time to 5 h resulted in fast transformation of zeolite A to sodalite phase, though a small amount of zeolite A was still present in SOD-0Et(5). The XRD pattern shows significantly intensified characteristic sodalite peaks and weakened zeolite A peaks (Fig. 1c). Different results were obtained from the XRD patterns of the samples prepared in the ethanol–water solvent system. Sodalite appears to be the only crystalline phase in the samples (Fig. 1d–g). Moreover, their XRD peaks were significantly broadened as compared with those prepared in the aqueous system, implying that the crystal sizes were much

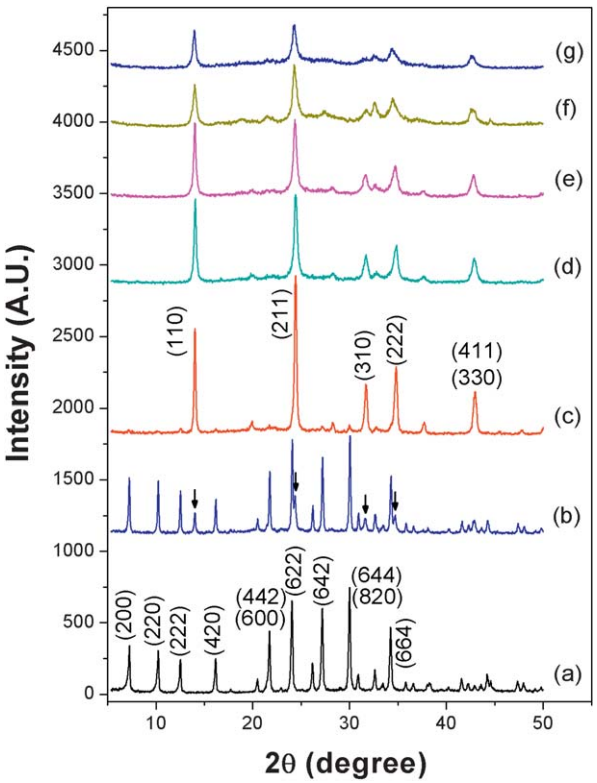

Fig. 1 XRD patterns of zeolite A (LTA) and sodalite (SOD) prepared with different amounts of water (Wt) and ethanol (Et) at 90 °C for $t = 3$–5 h. Spectra: (a) LTA-94Wt(3), (b) SOD-0Et(3), (c) SOD-0Et(5), (d) SOD-4Et(3), (e) SOD-8Et(3), (f) SOD-16Et(3), and (g) SOD-32Et(3). Spectra (a) and (c) are indexed to zeolite A and sodalite structures, respectively. The arrows in spectrum (b) indicate the emerging peaks of sodalite phase.

Table 1 Phases of the samples prepared in nC_2H_5OH (Et)–$3.61Na_2O$–$1Al_2O_3$–$1.20SiO_2$–$52.84H_2O$ and $3.61Na_2O$–$1Al_2O_3$–$1.20SiO_2$–$94H_2O$ (Wt) systems after different hydrothermal reaction times [a]

	Samples					
Time (h)	94Wt	0Et	4Et	8Et	16Et	32Et
1	Am-LTA	LTA-Am	LTA-Am	LTA-Am	Am	Am
2	LTA	LTA-SOD(T)	LTA-SOD	LTA-SOD	LTA-SOD	LTA-SOD
3	LTA	LTA-SOD	SOD-LTA(T)	SOD-LTA(T)	SOD-Am-LTA(T)	SOD*-LTA(T)
5	LTA	SOD-LTA(T)	SOD-LTA(T)	SOD/LTA(T)	SOD*	SOD*
8	LTA	SOD-LTA(T)	SOD	SOD	SOD*	SOD*
16	LTA	SOD	SOD	SOD	SOD	SOD*
25	LTA	SOD	SOD	SOD	SOD	SOD
45	LTA	SOD	SOD	SOD	SOD	SOD
65	LTA-SOD(T)	SOD	SOD	SOD	SOD	SOD

[a] The synthesis temperature is 90 °C; Am = amorphous materials; T = in trace amount; SOD* = sodalite with a trace amount of amorphous material.

smaller. Close examination of the XRD patterns from SOD-4/8/16/32Et(3) further revealed that the increase of ethanol content favored the crystallization of smaller sodalite crystals with gradually broadened characteristic sodalite peaks. However, it should be noted that by increasing the ethanol content, the final samples contain a slightly increased amount of amorphous material, as indicated by the gradually intensified halo area in the background ranging from 15° to 40°. This is probably because a slower crystal growth rate was obtained as more ethanol was involved in the synthesis, which is consistent with the work by Cheng and Shantz,[5] and Persson and co-workers.[33]

The morphology of each sample was studied using SEM and TEM. The LTA-94Wt(3) prepared in the water solvent system has a cubic morphology (Fig. 2a), the typical zeolite A morphology.[34,35] Zeolite A crystals in the sample possess particle sizes ranging from a couple of tens of nanometres to around 1 μm. Fig. 2b shows the SEM image of SOD-0Et(3) synthesized without addition of extra water and ethanol. As shown in the SEM image, it contains mainly rounded cubic crystals and a small proportion of disc-like clusters. Extension of the reaction time from 3 h to 5 h resulted in a substantial increase in the proportion of disc-like crystals (Fig. 2c and inset). According to the XRD result and phase transformation mechanism, the majority of the round cubic crystals in SOD-0Et(3) would be zeolite A phase whereas the disc-like crystals mainly contained in SOD-0Et(5) would be sodalite phase. It was also confirmed by selected area electron diffraction (SAED) examinations (ESI, Fig. S1a and b†). Interestingly, when a small amount of ethanol was added, abundant thread-ball-like particles with sizes about 0.5–2 μm were seen in the sample SOD-4Et(3) (Fig. 2d). TEM observations further confirmed that the thread-ball-like particle was composed of sodalite nano-plates (Fig. 2d, inset). When the amount of ethanol (designated $n_{ethanol}$, see experimental section) was increased to 8, smaller sodalite nano-plates with size about 80–150 nm were observed (Fig. 2e, and inset). Close views of the spherical particles revealed that a higher packing density of the sodalite nano-plates was produced (Fig. 2e inset), as opposed to those of SOD-0Et(5) and SOD-4Et(3). More TEM images and SAED patterns of the spherical sodalite particles from SOD-4Et (3) and SOD-8(3) are displayed in ESI, Fig. S1c and d.† Continuously increasing $n_{ethanol}$ to 16 led to the formation of core-shell sodalite particles with faceted sodalite nanocrystals (80–180 nm) packed densely at the shell and with smaller irregular crystals (<30 nm) at the core regions (arrows in Fig. 2f). TEM and SAED examinations of this sample confirm the polycrystalline nature of the core-shell nanostructure (Fig. 2f inset). In the system with a $n_{ethanol}$ value of 32, as shown in Fig. 2g and ESI Fig. S2† (high magnification SEM image), hierarchical particles with even smaller shell sodalite nanocrystals (20–80 nm) were synthesized. Close observations of those particles revealed that the building nanocrystals were highly crystalline. A typical high-resolution (HR) TEM image of the surface is presented in Fig. 2h, showing rounded cubic sodalite nanocrystals (~40 nm in size). The distinct lattice fringes shown in the image are extended along different directions, indicative of the overlap of several sodalite nanocrystals with different orientations. The SAED pattern taken on an entire particle also represents a characteristic polycrystalline SOD pattern (as indexed in Fig. 2h inset), confirming that the hierarchical particle is made of intergrown sodalite nanocrystals. From these SEM and HRTEM studies, it has been found that by increasing the proportion of ethanol, the system favored crystallization of smaller sodalite nanocrystals, which is in good agreement with the XRD study. In the meantime, the change of the morphology of sodalite particles from nano-plate assemblies to nanocrystal intergrown core-shell structure was observed. Additionally, SEM and TEM examinations on broken particles revealed that these particles have a core-shell structure with nanocrystalline shell crystals and a large amount of non-crystalline core material. The latter may serve as a nutrient reservoir for the shell crystal growth as the reaction time increased. The evolution of these core-shell particles to hollow sodalite architectures will be discussed in detail as follows.

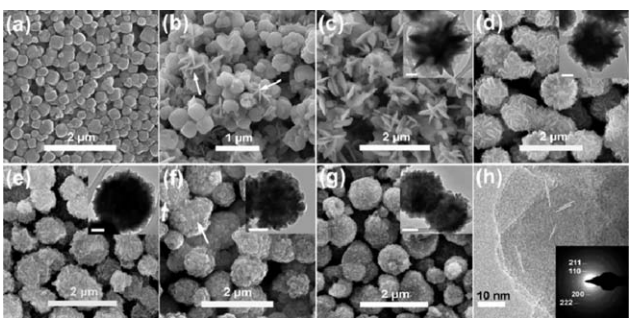

Fig. 2 SEM and TEM images of zeolite A (LTA) and sodalite (SOD) prepared with different amounts of water (Wt) and ethanol (Et). Panels: (a) LTA-94Wt(3), (b) SOD-0Et(3) (mainly zeolite A phase), (c) SOD-0Et (5) (mainly sodalite phase), (d) SOD-4Et(3), (e) SOD-8Et(3), (f) SOD-16Et(3), (g) SOD-32Et(3), and (h) HRTEM image of the particle surface in SOD-32Et(3). The insets in FIB-SEM (c)–(g) are TEM images showing the typical morphology of the particles in each sample. The scale bar for them is 200 nm. SAED pattern as shown in panel h was taken from the entire particle in sample SOD-32Et(3).

Sodalite crystallization at different stages of hydrothermal synthesis

To unveil the formation mechanism of the core-shell/hollow sodalite, specimens were collected after the crystal growth times of 0.5, 1, 2, 3, 5, 16, 25, 35, 45, and 65 h from the synthesis mixture with a molar composition of $16C_2H_6O : 3.61Na_2O : 1.00Al_2O_3 : 52.84H_2O : 1.20SiO_2$.

The XRD patterns of the specimens are shown in Fig. 3. After a reaction time of 0.5 h, the sample SOD-16Et(0.5) appeared to be amorphous (Fig. 3a). Continuously heating the synthesis mixture to 1 h still did not lead to any detectable crystalline phase (Fig. 3b). When the reaction time was extended beyond 2 h, the characteristic XRD pattern of zeolite A appeared (Fig. 3c). However, sodalite with much smaller crystal size had already formed as indicated by the broad diffraction peak at 2θ angle of ~14.15°. Diffraction peaks of zeolite A structure almost disappeared when the reaction time was 3 h. Instead, a well-defined sodalite diffraction pattern was obtained (Fig. 3d), indicating that fast phase transformation of zeolite A to sodalite took place between 2–3 h. Thermodynamically, phase transformation occurs due to higher stability of the denser sodalite lattice as compared to zeolite A.[31,36] Subotic and co-workers performed

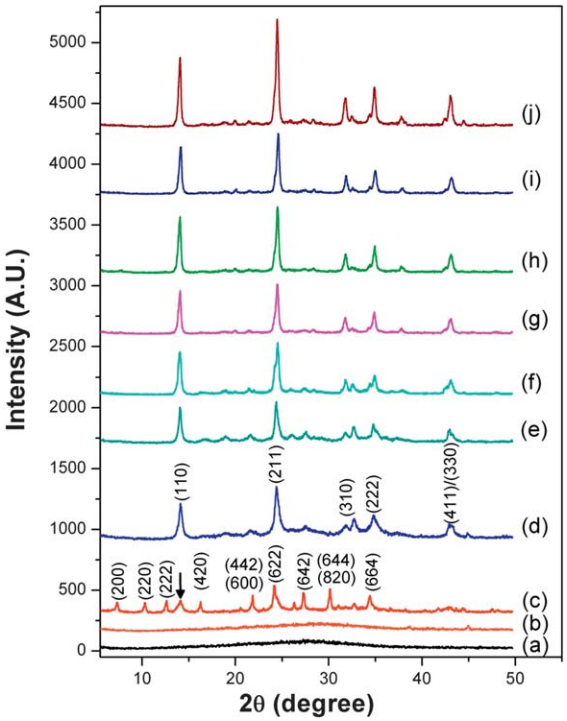

Fig. 3 XRD patterns of specimens SOD-16Et(t) prepared in the system with different hydrothermal reaction times (t): (a) $t = 0.5$, (b) $t = 1$, (c) $t = 2$, (d) $t = 3$, (e) $t = 5$, (f) $t = 16$, (g) $t = 25$, (h) $t = 35$, (i) $t = 45$ h, and (j) $t = 65$ h. Patterns (c) and (d) were indexed to zeolite A and sodalite phases, respectively. The black arrow in pattern (c) shows a weak peak of sodalite phase.

a comprehensive study of this phase transformation process and found that it was a solution-mediated process starting with the dissolution of zeolite A, followed by the supersaturation of the synthesis solution and then heterogeneous nucleation.[31] Our results suggest that this transformation mechanism is applicable during this period (2–3 h), since a certain amount of amorphous material is presumably produced *via* the dissolution of zeolite A, as indicated by the appearance of a broad background peak ranging from 15 to 40° in the XRD pattern (Fig. 3d). Moreover, the diffraction peaks are significantly broadened, implying that much smaller sodalite crystals were formed. With increasing the hydrothermal reaction times from 5 to 65 h, the diffraction peaks become more intense (Fig. 3 e–j), as expected from longer growth times. It is worth mentioning that the longer crystallization does not result in any other zeolite phase, implying that the present synthesis condition is favorable for sodalite crystallization.

A complementary Fourier transform infrared (FT-IR) study was performed on a series of specimens obtained in different crystal growth periods (see ESI Fig. S3†). The IR examinations revealed that a fast phase transformation from zeolite A to sodalite took place at the early growth stage (1–3 h), in good agreement with XRD results. As also indicated by IR study, a trace amount of zeolite A phase is present throughout 3 and 65 h reaction times under the present synthesis conditions. Consequently, no pure sodalite was ever produced at any stage, although the sodalite phase was dominant after a growth time of 3 h, as detected by XRD.

The morphologies of the specimens with different growth times were examined. It should be noted that for each growth time at least 6 specimens were prepared and examined. The representative SEM, FIB-SEM, and TEM images are displayed in Fig. 4–7. Fig. 4a shows that amorphous aluminosilicate gel particles with hierarchical porous structures formed after 0.5 h heating. The appearance of these highly porous structures would lead to a substantial increase of the liquid–solid (amorphous gel phase) interfacial areas, which has been considered to favor the surface-catalyzed heterogeneous nucleation.[8,9] After 1 h of reaction, the porous particles with globular shapes dominated in the sample (Fig. 4b). However, TEM and SAED examinations on these globular particles revealed that they were still non-crystalline. Note that some of them were in contact with half-ball-like particles with sizes ranging from a couple of hundreds of nanometres to around 1 μm (as indicated by the circle in Fig. 4b). The dense-packing surfaces of these spheres may be possible sites for heterogeneous surface-catalyzed nucleation. However, at this stage, no notable crystallization was observed, which was in good agreement with XRD and IR results.

After hydrothermal treatment for 2 h, both spherical and cubic particles were observed in the SEM (Fig. 4c) and FIB-SEM images (Fig. 5a). A slightly increased size of the spherical particles (0.2–1.5 μm) was also observed. Moreover, as shown in Fig. 5e, both spheres and cubes are solid without apparent core-shell structures. HRTEM image taken on the cubic particle show distinct lattice fringes with a measured d spacing of 12.5 Å, which matches the (200) plane in zeolite A (ESI Fig. S4†). The spherical particles with very rough surface gave a characteristic polycrystalline sodalite SAED pattern (Fig. 7a, inset). Closer examination on the rough surface further confirms the appearance of many nanocrystalline sodalite particles with sizes of around 20–80 nm near the surface (Fig. 7a). In addition, the fast Fourier transform (FFT) of the highlighted region of the HRTEM image of shell nanocrystals is consistent with sodalite structure indexed as the [111] zone axis (Fig. 7b and inset).

When the reaction time was increased to 3 h, the quantity of spherical sodalite particles substantially increased while the cubic

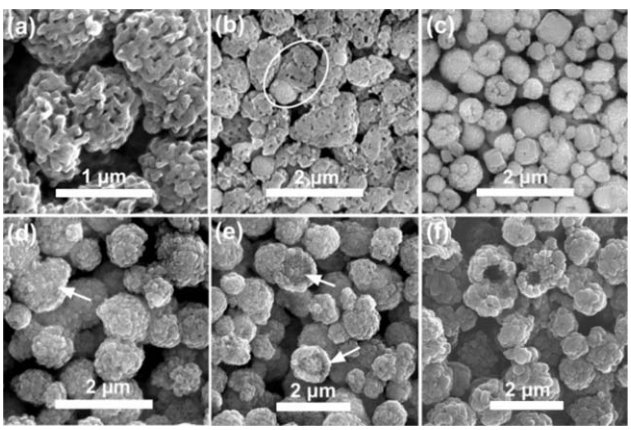

Fig. 4 SEM images of specimens SOD-16Et(t) after different crystal growth times. (a) $t = 0.5$, (b) $t = 1$, (c) $t = 2$, (d) $t = 3$, (e) $t = 16$, and (f) $t = 65$ h. The circle in panel b shows a submicron-sized sphere attaching to a porous gel particle. Arrows in panels d and e point to broken sodalite particles with apparent core-shell structures.

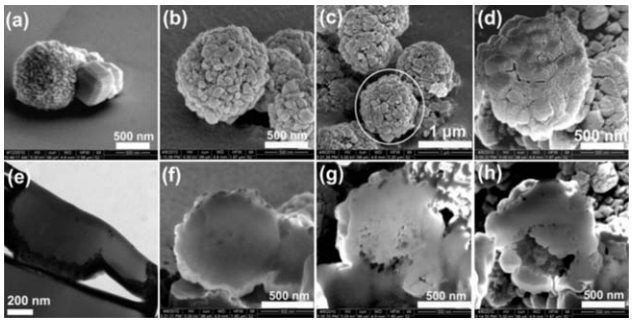

Fig. 5 SEM images (a–d) of entire particles SOD-16Et(t) before ion-beam milling: (a) $t = 2$, (b) $t = 3$, (c) $t = 16$, and (d) $t = 45$ h. TEM image (e) displays the cross-sectional profile of a spherical particle attached to a cubic zeolite A as shown in panel (a). Panels f–h are the corresponding FIB-SEM images of SOD-16Et(t): (f) $t = 3$, (g) $t = 16$, and (h) $t = 45$ h.

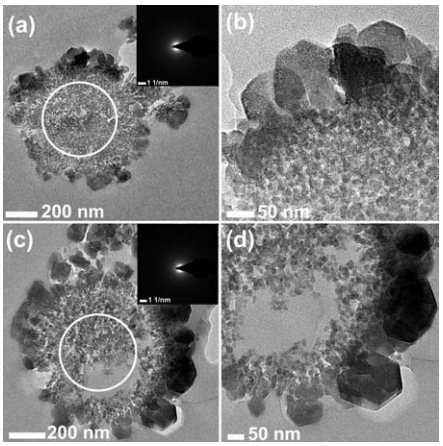

Fig. 6 TEM images of the sectioned sodalite particles with a thickness of 70 nm (a–b) SOD-16Et(3) and (c–d) SOD-14.5Et(16). Panels (b) and (d) are HR-TEM images showing the features near the core-shell boundaries. The SAED patterns were taken from the central core region (highlighted by the cycles) and displayed in the upper right of panels (a) and (c).

zeolite A particles were rarely observed during SEM/TEM imaging. This observation suggests that a fast phase transformation occurs between 2h and 3h, which is consistent with XRD results. The SEM (Fig. 4d and 5b) and TEM (Fig. 7c) images show that the spherical particles tend to coagulate with each other and their surfaces are covered by more faceted nanocrystals with sizes of around 80–180 nm. SAED examinations confirmed that these spherical sodalite particles are polycrystalline in nature (Fig. 7c inset). In addition, under dark-field (DF) TEM observation, plenty of bright contrast, arising from nanocrystalline sodalite, appears at the peripheries of the particles (Fig. 7d), which provides strong evidence for surface nucleation and crystallization. The representative FIB-SEM image (Fig. 5f) revealed that the spherical particle was solid, although the morphology of shell layer and core was not clearly observed due to charging effects on imaging. In order to view the detailed features of the cross-sectional profile of the sodalite particle and also protect the particle interior from the damage of dual beam high resolution focus ion beam (FIB) milling, the spherical sodalite particles were mechanically cut into a number of 70 nm thick sections before TEM examinations. TEM images of the

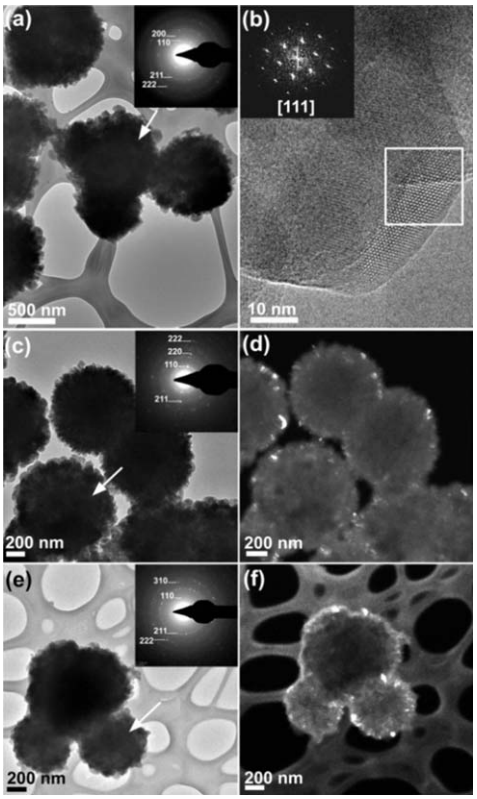

Fig. 7 TEM images of (a–b) SOD-16Et(2), (c–d) SOD-16Et(3), and (e–f) SOD-16Et(16). (b) is the HRTEM image captured on a shell sodalite nanocrystal. (d) and (f) are dark-field (DF) TEM images. The insets in panels (a), (c), and (e) are selected area electron diffraction (SAED) patterns collected from the entire particles as pointed by the arrows in each panel. The inset in panel (b) is the fast Fourier transform (FFT) pattern derived from the highlighted region in HRTEM image (b).

sectioned core-shell sodalite particles are shown in Fig. 6a, b. Sodalite nanocrystals with polyhedral morphology were clearly observed intergrown on the particle surfaces (Fig. 6a). The HRTEM image (ESI Fig. S5a†) also shows distinct sodalite lattice fringes with a d_{110} spacing of 6.25 Å, confirming that they have sodalite structure. However, the interior material with finely divided hierarchical structure appeared to be amorphous, as indicated by the SAED examinations (Fig. 6a, inset). Such hierarchical porous structure is commonly observed from the hard gel phase at an early stage of hydrothermal synthesis.[37,38] Moreover, HRTEM image (Fig. 6b) captured near the core-shell boundary revealed pronounced morphological difference between the shell crystals (crystalline phase) and the amorphous core (noncrystalline phase). These observations further confirm that the multiple nucleations instead of single nucleation on the amorphous surface occur at an early crystal growth stage. As shown in Fig. 7c, intermediate sodalite particles with compact packing of needle-like crystals (approx. 20 nm × 40 nm) on the surfaces are also present in the sample.

When the crystal growth time was extended to 16 h, the core-shell structure became more apparent as shown in the SEM image (Fig. 4e, pointed by arrows) and representative FIB-SEM image (Fig. 5g). During this period, most surface crystals grew to over 100 nm in size but the overall particle sizes remained at 0.5–1.8 μm (Fig. 4e and 5c). Extensive TEM examinations on the

sectioned particles (Fig. 6c, d, and ESI Fig. S6†) as well as the entire spherical particles (Fig. 7e, f) revealed that the shell crystals with apparent polyhedral morphology were highly crystallized and well intergrown at this stage, forming a polycrystalline shell with a thickness of around 150 nm. However, their interior space was still filled with very fine amorphous particles (Fig. 6, inset) similar to those observed from sample SOD-14.5Et(3). It is noted that the core was partially consumed at this stage, leaving large cavities near the core-shell boundary (Fig. 6d). The phenomena observed here, surface crystallization and amorphous core consumption process, are in good agreement with the surface-to-core crystallization process as reported earlier by several groups.[12–14]

Further prolongation of crystallization time led to the core digestion process. A significantly reduced amount of interior material was observed as the heating time was increased to 45 h (Fig. 4f). A representative FIB-SEM image (Fig. 5h) from the 45 h heated sample revealed the nutrients near the interior surface were preferentially consumed, leaving large cavities between the shell and the core. A small increase in the shell thickness to about 250 nm was also observed. Sodalite particles with almost hollow cores were developed after 65 h. SEM and FIB-SEM images showing the typical morphology of the hollow sodalite with bumpy interior surfaces is shown in ESI Fig. S7.† The extensive SEM observations on a number of hollow sodalite particles revealed that many shell crystals significantly grew to over 200 nm in size. Importantly, most of the shell crystals show a polyhedral morphology which is completely different to the "nanorod" intermediates observed in the formation of hollow sodalite spheres reported in our previous work.[15] It is also worth mentioning that the overall dimensions of the spherical particles in most of the specimens are fairly similar (0.5–2 μm), while the shell crystals grew significantly from 10–30 nm (3 h, Fig. 4d and 5b) to 100–250 nm (45 h, Fig. 4f and 5d) at the expense of nutrients in the solution and the amorphous core of spherical particles, which is strong evidence for surface crystallization and amorphous core consumption process processes. According to our experimental results, the surface crystallization phenomenon was also observed in the system with higher ethanol content ($n_{ethanol} = 32$). However, the spherical sodalite particles after the same hydrothermal synthesis time (*e.g.*, SOD-32Et(3)) contained much smaller shell-crystals (~40 nm) as compared with SOD-16Et(3), probably due to the decreased crystal growth in presence of more ethanol. More TEM analysis of this sample is reported in ESI Fig. S8–9† and discussed in more detail therein.

The core-shell/hollow sodalite samples SOD-16Et(t) with different reaction times (*e.g.*, $t = 3$, 25, 45, and 65 h) were also studied by thermogravimetric (TG) analysis in air and nitrogen (ESI Fig. S10†). The TG results indicated that a small amount of ethanol (~1 wt%) remained in the samples after repeatedly washing and drying. Moreover, the decomposition of ethanol was observed in a higher and broader temperature range (350–500 °C), as compared to the combustion of structural ethanol in other zeolite (200–450 °C), such as MFI-type zeolite.[22] This result implies the interaction between ethanol and sodalite structure is much stronger under current synthesis conditions.

Based on the results presented above, it is concluded that the formation of core-shell/hollow sodalite particles in our system involves formation of amorphous aggregates, surface multi-nucleation, and solution-mediated crystal growth and intergrowth on the surface to increase the shell thickness by consuming the nutrients in the system (*e.g.*, in the core and external liquid). Hollow spherical polycrystalline sodalite particles were formed when the particle interiors were completely consumed.

Formation mechanism of core-shell/hollow sodalite in the ethanol–Na_2O–Al_2O_3–SiO_2–H_2O system

Our studies on the synthesis of sodalite with different amounts of ethanol and detailed examinations of the core-shell/hollow sodalite formation process allow us to gain some useful insight into the effects of ethanol on crystallization. In the present work, the addition of ethanol has been observed to considerably alter the physical properties of the zeolite gel, such as density. This phenomenon has been verified by a series of control experiments, and the details are presented in ESI Fig. S11.† The increase of ethanol content in the synthesis mixture led to the formation of denser zeolite gel which partitioned into the bottom of synthesis solution. Note that the condensation process would simultaneously enhance the degree of the supersaturation of zeolite gel phase, which increases the nucleation rate.[39,40] Zeolite crystallization kinetics would be considerably accelerated, leading to large sodalite crystals. However, after the activity of reactive species reaches the maximum, further addition of ethanol would lead to further dilution of the system (*i.e.*, lower system alkalinity) and consequently produce lower crystallization rate. At the crystal growth stage, an aggregation mechanism dominates and governs the crystal growth and aggregation,[10,11] leading to the formation of hierarchical sodalite nanostructures. Based on our experimental results, sodalite nano-plate aggregates are formed in the synthesis system with a low ethanol content (12–26 wt% ($n_{ethanol} = 4$–8) of the entire synthesis mixture) whereas core-shell/hollow sodalite nanostructures are produced at a high ethanol proportion of 35–70 wt% ($n_{ethanol} = 16$–48). The staged observations of the synthesis in the presence of ethanol ($n_{ethanol} = 16$) revealed that the zeolite crystallization followed the multi-nucleation and crystallization on the surface. At an early stage (0–1 h), zeolite gel agglomerated, forming hierarchical porous structures, followed by a fast crystallization of zeolite A (1–2 h). The crystallization of zeolite A under current hydrothermal conditions follows the heterogeneous nucleation—solution-mediated crystal growth.[9,35,40–42] In the same period, sodalite phase appeared starting with amorphous spherical particles (~1 h). Probably owing to the strong interaction between ethanol and the inorganic gel solid, the spherical particle surface presumably served as ideal nucleation sites, where numerous protozeolite nuclei formed rapidly. Sodalites then quickly grew on the surfaces, forming a thin polycrystalline shell with an amorphous core (2 h). Unfortunately, we are unable to identify the first zeolite phase (zeolite A or sodalite) appearing in the sample at early crystal growth stage (1–3 h) due to the very fast nucleation and crystallization kinetics in the current system. However, based on our results, we tend to believe the phase transformation from zeolite A to sodalite follows a solution-mediated process in which zeolite A fast dissolved to form the nutrients (*e.g.*, solvated aluminosilicates species) for the surface crystallization of the amorphous spherical particles. Other

mechanisms such as secondary nucleation of sodalite in zeolite A amorphous cores[12] and solid to solid transformation of zeolite A to sodalite[43] were not observed in the present work. In the next growth stage (3–16 h), an apparent core-shell structure of the spherical particles was developed with more faceted sodalite crystals intergrown on the surface. Further extension of the reaction time (16–45 h) led to the core digestion and increase in shell thickness. Hollow sodalites with intergrown polyhedral shell crystals can be synthesized after a reaction time of 65 h. This surface crystallization and core consumption process is similar to the previously observed cases in zeolite A[12,13] and zeolite analcime.[14]

The surface multi-nucleation and crystallization was also observed when even more ethanol ($n_{ethanol} = 32$) was present. However, nanocrystalline sodalites with much smaller sizes were crystallized on the surface of amorphous spherical particles after a growth time of 3 h. This result again confirms that further dilution of the system through the addition of more ethanol ($n_{ethanol} > 16$) to the synthesis solution gives lower crystallization rate in the system which favours the formation of sodalite with smaller crystal sizes. However, how ethanol affects zeolite crystallization at the molecular scale is still unclear. It has been reported that ethanol molecule favors the interfacial positions of the water clathrate framework which was formed around the cation (*e.g.*, Na^+) during hydrophobic hydration.[5,44–46] It has been also proposed that the effective interchange of the clathrate water molecules and reactive aluminosilicate species is one of the factors in zeolite growth.[47,48] In this regard, decreased mass transport rate might be related to the slower exchange rate of solvated reactive aluminosilicate species and clathrate water molecules around the cation due to the strong interaction between ethanol and water molecules. More ethanol in the system probably further slows down the interchange efficiency, resulting in a decreased crystal growth rate. Sodalites with smaller shell crystals were thus synthesized for the same synthesis period.

The surface crystallization mechanism may not be unique to sodalite and the ethanol-water solvent system. It may be a common phenomenon in the alcohol-water solvent system. By using different alcohols (*e.g.*, methanol, butanol, propanol) and zeolite gel composition, it could be possible to fabricate other zeolites (*e.g.*, FAU/LTL/BEA-type zeolite) with novel nanostructures *via* a similar crystallization process. Moreover, the method described here does not involve the use of a hard template, and thus is very effective for the facile synthesis of nanostructured zeolite materials.

4. Conclusions

We have shown that sodalite particles with different morphologies and size distributions can be synthesized by varying the ethanol content in the organic-SDA-free system. Ethanol plays an important role in affecting the crystal growth kinetics and final zeolite morphologies. Particularly, when high proportions of ethanol ($n_{ethanol} = 16–32$) are involved, surface crystallization takes place, *i.e.*, multi-nucleation and solution-mediated crystal growth/intergrowth occur on the surface of the amorphous spherical particles, and then extend inwards to increase the shell thickness at the expense of the nutrients in the system. Hollow sodalite particles with polycrystalline shell layer were synthesized once all nutrients in the core are consumed.

Acknowledgements

Financial support from the CSIRO Water for a Healthy Country Flagship and Australian Research Council (ARC) is greatly acknowledged. Y.H. thanks the CSIRO for the postgraduate scholarship. J.Y. thanks Monash University for the Monash Fellowship. H.W. thanks the ARC for the Future Fellowship. M. H. and A.H. acknowledge support from the CSIRO OCE Science Leader Scheme. X.Z. and M.T. gratefully acknowledge partial financial support from the Petroleum Institute of Abu Dhabi through the ADMIRE (Abu Dhabi – Minnesota Institute for Research Excellence) partnership and from IREE. Part of this work was carried out in the Characterization Facility at the University of Minnesota, a member of the NSF-funded Materials Research Facilities Network (www.mrfn.org) *via* the MRSEC program.

Notes and references

1 R. M. Barrer, *Zeolite and Clay Minerals as Sorbents and Molecular Sieves*, Academic Press, London, 1978.
2 R. M. Barrer, *Hydrothermal Chemistry of Zeolites*, Academic Press, London, 1982.
3 T. Bein, *Chem. Mater.*, 1996, **8**, 1636–1653.
4 D. W. Breck, *Zeolite Molecular Sieves: Structure, Chemistry and Use*, John Wiley & Sons, New York, 1974.
5 C. H. Cheng and D. F. Shantz, *J. Phys. Chem. B*, 2005, **109**, 19116–19125.
6 M. E. Davis, *Ind. Eng. Chem. Res.*, 1991, **30**, 1675–1683.
7 M. E. Davis and R. F. Lobo, *Chem. Mater.*, 1992, **4**, 756–768.
8 V. Nikolakis, D. G. Vlacho and M. Tsapatsis, *Microporous Mesoporous Mater.*, 1998, **21**, 337–346.
9 V. P. Valtchev and K. N. Bozhilov, *J. Am. Chem. Soc.*, 2005, **127**, 16171–16177.
10 Y. Huang, K. Wang, D. H. Dong, D. Li, M. R. Hill, A. J. Hill and H. T. Wang, *Microporous Mesoporous Mater.*, 2010, **127**, 167–175.
11 V. P. Valtchev and K. N. Bozhilov, *J. Phys. Chem. B*, 2004, **108**, 15587–15598.
12 H. Greer, P. S. Wheatley, S. E. Ashbrook, R. E. Morris and W. Z. Zhou, *J. Am. Chem. Soc.*, 2009, **131**, 17986–17992.
13 J. F. Yao, D. Li, X. Y. Zhang, C. H. Kong, W. B. Yue, W. Z. Zhou and H. T. Wang, *Angew. Chem., Int. Ed.*, 2008, **47**, 8397–8399.
14 X. Chen, M. Qiao, S. Xie, K. Fan, W. Zhou and H. He, *J. Am. Chem. Soc.*, 2007, **129**, 13305–13312.
15 L. Han, J. F. Yao, D. Li, J. Ho, X. Y. Zhang, C. H. Kong, Z. M. Zong, X. Y. Wei and H. T. Wang, *J. Mater. Chem.*, 2008, **18**, 3337–3341.
16 Q. Wang, G. Chen and S. Xu, *Microporous Mesoporous Mater.*, 2009, **119**, 315–321.
17 Y. Huang, D. H. Dong, J. F. Yao, L. He, J. Ho, C. H. Kong, A. J. Hill and H. T. Wang, *Chem. Mater.*, 2010, **22**, 5271–5278.
18 S. Mintova, N. H. Olson, V. Valtchev and T. Bein, *Science*, 1999, **283**, 958–960.
19 T. M. Davis, T. O. Drews, H. Ramanan, C. He, J. S. Dong, H. Schnablegger, M. A. Katsoulakis, E. Kokkoli, A. V. McCormick, R. L. Penn and M. Tsapatsis, *Nat. Mater.*, 2006, **5**, 400–408.
20 H. T. Wang, Z. B. Wang and Y. S. Yan, *Chem. Commun.*, 2000, 2333–2334.
21 E. Costa, M. A. Uguina, A. Delucas and J. Blanes, *J. Catal.*, 1987, **107**, 317–324.
22 X. L. Seoane, A. Arcoya, J. A. Gonzalez and N. Travieso, *J. Mater. Sci.*, 1991, **26**, 172–176.
23 W. Song, R. E. Justice, C. A. Jones, V. H. Grassian and S. C. Larsen, *Langmuir*, 2004, **20**, 8301–8306.

24 M. A. Uguina, A. Delucas, F. Ruiz and D. P. Serrano, *Ind. Eng. Chem. Res.*, 1995, **34**, 451–456.
25 S. Mintova, N. H. Olson and T. Bein, *Angew. Chem., Int. Ed.*, 1999, **38**, 3201–3204.
26 H. T. Wang, Z. B. Wang, L. M. Huang, A. Mitra and Y. S. Yan, *Langmuir*, 2001, **17**, 2572–2574.
27 C. S. Carr and D. F. Shantz, *Microporous Mesoporous Mater.*, 2005, **85**, 284–292.
28 C. S. Carr and D. F. Shantz, *Chem. Mater.*, 2005, **17**, 6192–6197.
29 J. F. Yao, L. X. Zhang and H. T. Wang, *Mater. Lett.*, 2008, **62**, 4028–4030.
30 M. M. J. Treacy, J. B. Higgins, *Collection of Simulated XRD Powder Pattern for Zeolites*, Elsevier, London, 2007.
31 B. Subotic, D. Skrtic, I. Smit and L. Sekovanic, *J. Cryst. Growth*, 1980, **50**, 498–508.
32 R. I. Walton, F. Millange, D. O'Hare, A. T. Davies, G. Sankar and C. R. A. Catlow, *J. Phys. Chem. B*, 2001, **105**, 83–90.
33 A. E. Persson, B. J. Schoeman, J. Sterte and J. E. Ottesstedt, *Zeolites*, 1994, **14**, 557–567.
34 C. Kosanovic, T. A. Jelic, J. Bronic, D. Kralj and B. Subotic, *Microporous Mesoporous Mater.*, 2011, **137**, 72–82.
35 A. Palcic, J. Bronic, D. Brlek and B. Subotic, *CrystEngComm*, 2011, **13**, 1215–1220.
36 D. J. Wang, Y. H. Zhang, A. G. Dong, Y. Tang, Y. J. Wang, J. C. Xia and N. Ren, *Adv. Funct. Mater.*, 2003, **13**, 563–567.
37 W. Fan, K. Morozumi, R. Kimura, T. Yokoi and T. Okubo, *Langmuir*, 2008, **24**, 6952–6958.
38 M. Tsapatsis, M. Lovallo and M. E. Davis, *Microporous Mater.*, 1996, **5**, 381–388.
39 R. W. Thompson and A. Dyer, *Zeolites*, 1985, **5**, 292–301.
40 J. Warzywoda and R. W. Thompson, *Zeolites*, 1989, **9**, 341–345.
41 B. Subotic, in *ACS Symposium Series*, 1989, pp. 110–123.
42 S. Bosnar, J. Bronic, I. Krznaric and B. Subotic, *Croat. Chem. Acta*, 2005, **78**, 1–8.
43 L. H. Ding, H. Yang, P. Rahimi, O. Omotoso, W. Friesen, C. Fairbridge, Y. Shi and S. Ng, *Microporous Mesoporous Mater.*, 2010, **130**, 303–308.
44 S. Dixit, J. Crain, W. C. K. Poon, J. L. Finney and A. K. Soper, *Nature*, 2002, **416**, 829–832.
45 F. Franks and D. J. G. Ives, *Q. Rev. Chem. Soc.*, 1966, **20**, 1–44.
46 J. Turner and A. K. Soper, *J. Chem. Phys.*, 1994, **101**, 6116–6125.
47 S. L. Burkett and M. E. Davis, *J. Phys. Chem.*, 1994, **98**, 4647–4653.
48 S. L. Burkett and M. E. Davis, *Chem. Mater.*, 1995, **7**, 1453–1463.

